Transmission-Line Model for Field-to-Wire Coupling in Bundles of Twisted-Wire Pairs Above Ground

Giordano Spadacini, *Member, IEEE*, Flavia Grassi, *Senior Member, IEEE*, Filippo Marliani, and Sergio A. Pignari, *Fellow, IEEE*

I. Introduction

CABLES composed of twisted-wire pairs (TWPs) bundled together to form tightly packed harnesses are commonly used in aerospace applications for the interconnection of units integrated in the final system. Due to possible coupling with external electromagnetic fields, these cables represent a possible path for the propagation of interference to terminal units [1]. Since system-level testing in the development cycle is often bounded by severe schedule constraints, the availability of radiated susceptibility (RS) computational models at early design stages to predict potential problems and optimize the layout of the system (e.g., the cable routes) is of paramount importance to avoid after-the-fact remedial measures implying significant costs.

Though full-wave numerical methods, such as the method of moments (MoM) or the finite integration technique are very accurate, they would require an excessive computational burden for meshing cables installed in large systems. Hence, state-of-the-art approaches to the prediction of RS are based on the multiconductor transmission-line (MTL) theory [2]–[5]. According to these approaches, full-wave codes are used in a first stage to compute the *incident* electromagnetic field *in the absence of the cables*. Subsequently, field-to-wire coupling models based on the MTL are used to evaluate the propagation of the induced noise along the cables and in terminal loads.

For the analysis of *nonuniform* cables (i.e., those having variable cross section), the solution process is generally based on the approximation of the MTL as the cascade of *uniform* sections [6]. Specifically, for the prediction of crosstalk in bundles composed of TWPs, this approach was used in [7], where the MTL was subdivided into half-twist sections, and in [8], where a finer segmentation into $6-50$ sections per twist was proposed. Given the short length of the twist pitch in common applications (less than a few centimeters), the use of a dense segmentation would significantly increase the computational burden required for modeling long cable harnesses.

However, as shown in [9] and [10], for modeling the response of a single TWP driven by a plane-wave field, such an onerous subdivision into uniform sections can be avoided by defining an equivalent MTL having per-unit-length (p.u.l.) parameters averaged over the twist pitch, i.e., the spatial period of wire twisting. Furthermore, since the two wires in the TWP lie on average at the same height above ground, common-mode (CM) excitation is often the dominant effect in the field-coupling mechanism, whereas the differential mode (DM) noise can be mainly ascribed to CM-to-DM conversion due to system imbalance [11]–[15].

These are the fundamental assumptions involved in the derivation of the model proposed in this paper, which extends RS analysis to bundles of TWPs running above the ground. Moreover, the proposed MTL model allows for a nonuniform electromagnetic field impinging the bundle, sampled along the line, yielding prediction of the voltages and currents induced at the terminations of each wire in the bundle. The obtained quantities are then postprocessed by introducing CM and DM voltages/currents for each TWP, so to provide the designer with practical estimates of the CM and DM noise the terminal devices of each differential interconnect could be subject to.

This paper is outlined as follows. Section II presents the averaged p.u.l. parameter for a bundle of TWPs, leading to the definition of an equivalent uniform MTL. In Section III, a field-to-wire coupling model is then derived with reference to a nonuniform electromagnetic field sampled along the cable bundle. Several simulations reported in Section IV are compared versus independent full-wave MoM solutions to assess the accuracy,

Manuscript received December 3, 2013; revised March 7, 2014; accepted May 11, 2014. Date of publication May 21, 2014; date of current version December 11, 2014.

G. Spadacini, F. Grassi, and S. A. Pignari are with the Department of Electronics, Information and Bioengineering, Politecnico di Milano, 20133 Milan, Italy (e-mail: giordano.spadacini@ polimi.it; flavia.grassi@ polimi.it; sergio.pignari@ polimi.it).

F. Marliani is with the European Space Research and Technology Centre, European Space Agency, 2201 AZ Noordwijk, The Netherlands (e-mail: filippo.marliani@esa.int).

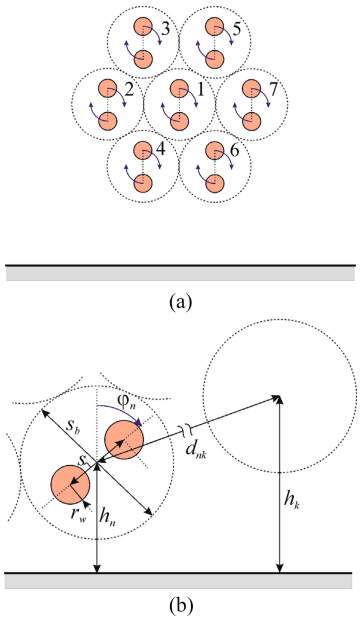

Fig. 1. Cross section of the cable bundle: (a) seven TWPs arranged in pseudo-circular form and (b) definition of geometrical parameters.

limits of validity, and computational efficiency of the model. Additionally, it is shown that the CM noise substantially differs from a TWP to another in the bundle, depending on the relative positions assumed in the cross section. Finally, Section V draws concluding remarks.

II. Bundle of TWPs

A. Structure Under Analysis

The structure under analysis is a cable bundle composed of an arbitrary number *N* of TWPs (without loss of generality, seven TWPs are exemplified here) running above a perfectly conducting ground.

Since the two wires forming each TWP are wound into a bifilar helix, the cross section of the structure is variable. However, by assuming that relative positions of TWP axes are invariant, a cross section for the whole bundle can be represented as shown in Fig. 1(a), where each TWP is sketched as a rotating wire-pair enclosed in a fixed circular region (dashed circle). Such regions are tightly packed and arranged in pseudocircular form.

The involved geometrical parameters are defined in Fig. 1(b). Namely, the wire radius r_w, wire separation s, and pair separation in the bundle s_b are common to all TWPs. Conversely, h_n is the height above the ground for the *n*th TWP, and d_{nk} is the distance between the *n*th and the *k*th TWP. Finally, the variable position of the *n*th pair can be identified by a tilt angle φ_n.

It is worth mentioning that in real-world TWP bundles, separations s and s_b are determined, to a large extent, by the thickness of the dielectric insulation surrounding each wire and by the possible presence of dielectric fillers. However, lossless bare wires are considered here to ease the development of the proposed model. The impact of neglecting the dielectric coating is investigated in Section IV-C.

B. Per-Unit-Length Parameters

By extending the approach used in [9] and [16] for modeling a single TWP, the *nonuniform* MTL is treated as an equivalent *uniform* MTL with *constant*, *averaged*, p.u.l. parameters. Rationale for this assumption is based on the ideal symmetry and balancing ensuing from wire twisting.

Specifically, the inductance matrix $\boldsymbol{L}$ is assumed to have the following super balanced structure:

$$\boldsymbol{L} = \begin{array}{c} \overbrace{}^{1}\ \overbrace{}^{2}\ \overbrace{}^{\cdots}\ \overbrace{}^{N} \\ \left[\begin{array}{cccccccc} \bar{l}_1 & \bar{l}_{M,1} & \bar{l}_{12} & \bar{l}_{12} & \dots & \dots & \bar{l}_{1N} & \bar{l}_{1N} \\ \bar{l}_{M,1} & \bar{l}_1 & \bar{l}_{12} & \bar{l}_{12} & \dots & \dots & \bar{l}_{1N} & \bar{l}_{1N} \\ \bar{l}_{12} & \bar{l}_{12} & \bar{l}_2 & \bar{l}_{M,2} & \dots & \dots & \bar{l}_{2N} & \bar{l}_{2N} \\ \bar{l}_{12} & \bar{l}_{12} & \bar{l}_{M,2} & \bar{l}_2 & \dots & \dots & \bar{l}_{2N} & \bar{l}_{2N} \\ \dots & \dots & \dots & \dots & \dots & \dots & \dots & \dots \\ \dots & \dots & \dots & \dots & \dots & \dots & \dots & \dots \\ \bar{l}_{1N} & \bar{l}_{1N} & \bar{l}_{2N} & \bar{l}_{2N} & \dots & \dots & \bar{l}_N & \bar{l}_{M,N} \\ \bar{l}_{1N} & \bar{l}_{1N} & \bar{l}_{2N} & \bar{l}_{2N} & \dots & \dots & \bar{l}_{M,N} & \bar{l}_N \end{array}\right] \begin{array}{l} \}1 \\ \\ \}2 \\ \\ \}\dots \\ \\ \}N \end{array} \end{array} \tag{1}$$

where $\bar{l}_n$ and $\bar{l}_{M,n}$ are the averaged self-inductance and mutual inductance of the wires belonging to the *n*th TWP, respectively, and $\bar{l}_{nk}$ is the averaged mutual inductance between a wire belonging to the *n*th TWP and a wire belonging to the *k*th TWP.

Averaging of p.u.l. inductances is intended over a twisting period, that is,

$$\bar{l}_n = \frac{1}{2\pi}\int_0^{2\pi} l_n(\varphi_n)\, d\varphi_n \tag{2}$$

$$\bar{l}_{M,n} = \frac{1}{2\pi}\int_0^{2\pi} l_{M,n}(\varphi_n)\, d\varphi_n \tag{3}$$

$$\bar{l}_{nk} = \frac{1}{4\pi^2}\int_0^{2\pi}\int_0^{2\pi} l_{nk}(\varphi_n,\varphi_k)\, d\varphi_n d\varphi_k \tag{4}$$

where $l_n(\varphi_n), l_{M,n}(\varphi_n), l_{nk}(\varphi_n,\varphi_k)$ are variable p.u.l. inductances depending on tilt angles. Though in general (2)–(4) can be accurately evaluated by numerical methods, suitable closed-form expressions can also be obtained under simplifying assumptions which are generally satisfied in practical cases. Namely, for widely separated wires [2], i.e., $s \geq 4r_w$, $s_b \geq s + 4r_w$, and under the additional constraint $h_n \geq 3s, \forall n$, a suitable analytical procedure (see the Appendix) leads to the approximate expressions

$$\bar{l}_n = \frac{\mu_0}{2\pi}\left[\ln\left(\frac{2h_n}{r_w}\right) - \frac{s^2}{16h_n^2}\right] + o[(s/h_n)^3] \tag{5}$$

$$\bar{l}_{M,n} = \frac{\mu_0}{2\pi}\left[\ln\left(\frac{2h_n}{s}\right) + \frac{s^2}{16h_n^2}\right] + o[(s/h_n)^4] \tag{6}$$

$$\bar{l}_{nk} = \frac{\mu_0}{4\pi}\ln\left(1 + \frac{h_n h_k}{d_{hk}^2}\right) + o[(s/d_{nk})^3] \tag{7}$$

where μ_0 is the magnetic permeability of vacuum, and $o(\cdot)$ indicates negligible terms (depending on third or greater powers of small adimensional parameters).

Finally, for the evaluation of the p.u.l. capacitance matrix $\boldsymbol{C}$, the assumption of homogeneous medium leads to

$$\boldsymbol{C} = c_0^{-2}\boldsymbol{L}^{-1} \tag{8}$$

where c_0 is the speed of light in the free space. The resulting structure of $\boldsymbol{C}$ is super balanced like for $\boldsymbol{L}$ in (1).

III. RS Model

The bundle running the above ground defined in Section II is now considered as a part of a more complex electromagnetic environment characterized by the presence of field sources, metallic surfaces, dielectric bodies, etc. This is the general framework of RS problems arising in industrial applications, such as cables installed inside a spacecraft. The aim of the following analysis is the derivation of a computationally efficient MTL model for the prediction of voltage/currents induced at terminal loads by a nonuniform electromagnetic field.

A. Sampling of the Incident Electromagnetic Field

The *incident* electromagnetic field, which is generated by field sources at the bundle position *with the bundle removed* [2], can be efficiently computed by means of analytical models in simple canonical cases [19], or via numerical full-wave solvers for complex electromagnetic environments. Therefore, it is assumed that a set of incident electric field values is known in a discretized space.

More exactly, the whole bundle is subdivided into N_S sections having (possibly different) lengths $\mathscr{L}_i, i = 1, 2, \ldots, N_\mathrm{S}$. Though the choice of lengths $\mathscr{L}_i$ is arbitrary, it should be consistent with the frequency-dependent nonuniformity of the field. As a rule of thumb, a good sampling scheme should ensure $\mathscr{L}_i < \lambda/20$, where λ is the wavelength, provided that the bundle is in the far-field region of the field sources. More restrictive conditions may apply for highly nonuniform fields in the near-field region of field sources, or in resonating environments [17]. Anyway, it is worth remarking that these requirements for the segmentation are not so severe as those correlated with wire twisting and involved in some models cited in Section I [7], [8].

The *i*th section of the bundle is represented as a filament running at $x = h$ above the ground in the local Cartesian reference system (*x*, *y*, *z*) shown in Fig. 2, where *h* is the height of the bundle axis, that is, the average value of all TWP heights (e.g., $h = h_1$ in Fig. 1). Within this bundle section, the following field quantities are sampled:

1) The real parts $E_{x,\mathrm{RE}}(0)$, $E_{x,\mathrm{RE}}(\mathscr{L}_i)$ and the imaginary parts $E_{x,\mathrm{IM}}(0)$, $E_{x,\mathrm{IM}}(\mathscr{L}_i)$ of the vertical component of the incident electric field evaluated for $x = h$, at $z = 0$ and $z = \mathscr{L}_i$, respectively.
2) The real parts $E_{z,\mathrm{RE}}(0)$, $E_{z,\mathrm{RE}}(\mathscr{L}_i)$ and the imaginary parts $E_{z,\mathrm{IM}}(0)$, $E_{z,\mathrm{IM}}(\mathscr{L}_i)$ of the longitudinal component of the incident electric field evaluated for $x = h$, and at $z = 0$ and $z = \mathscr{L}_i$, respectively.

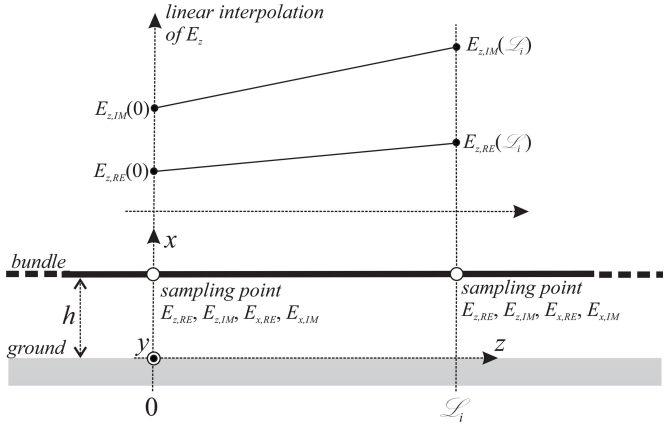

Fig. 2. Sampling of the nonuniform electromagnetic field along the bundle.

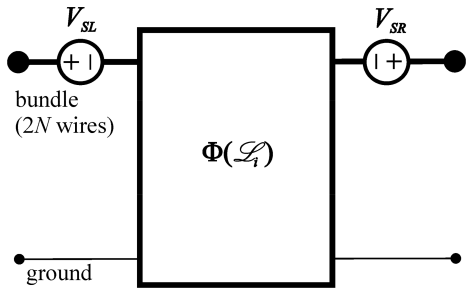

Fig. 3. Circuit model (at the external ports) of the *i*th bundle section.

B. Field-to-Wire Coupling Model

By applying the Agrawal field-to-wire coupling model [3] to the uniform MTL defined in Section II-B, together with an equivalent-circuit representation at external ports, the *i*th bundle section can be modeled as shown in Fig. 3. Namely, in this figure, the central block represents the chain-parameter matrix of a lossless MTL with length $\mathscr{L}_i$, that is

$$\boldsymbol{\Phi}(\mathscr{L}_i) = \begin{bmatrix} \cos(\beta_0\mathscr{L}_i)\mathbf{1}_{2N\times 2N} & -j\mathbf{Z}_\mathbf{C}\sin(\beta_0\mathscr{L}_i) \\ -j\mathbf{Z}_\mathbf{C}^{-1}\sin(\beta_0\mathscr{L}_i) & \cos(\beta_0\mathscr{L}_i)\mathbf{1}_{2N\times 2N} \end{bmatrix} \tag{9}$$

where $\boldsymbol{Z}_\mathbf{C} = c_0\boldsymbol{L}$, $\beta_0 = \omega/c_0$, ω is the angular frequency, and $\mathbf{1}_{2N}$ is the *2N* identity matrix. The thick line in Fig. 3 is an abstract representation of the 2*N* wires, carrying two voltage sources $\boldsymbol{V_{SL}}$ and $\boldsymbol{V_{SR}}$, at the left and right end, respectively, accounting for field-coupling effects.

Since the focus is on the CM, the incident electric field required for voltage-source evaluation according to the Agrawal model is assumed equal for both wires of each TWP, and evaluated in correspondence with the TWP axis. As a consequence, the source vectors of 2*N* elements assume the following

structure:

$$\boldsymbol{V_{SL}}=\begin{bmatrix} V_{\mathrm{SL},1} \\ V_{\mathrm{SL},1} \\ V_{\mathrm{SL},2} \\ V_{\mathrm{SL},2} \\ \dots \\ \dots \\ V_{\mathrm{SL},N} \\ V_{\mathrm{SL},N} \end{bmatrix} \begin{matrix} \\ \} 1 \\ \\ \} 2 \\ \\ \} \dots \\ \\ \} N \end{matrix} \quad \boldsymbol{V_{SR}}=\begin{bmatrix} V_{\mathrm{SR},1} \\ V_{\mathrm{SR},1} \\ V_{\mathrm{SR},2} \\ V_{\mathrm{SR},2} \\ \dots \\ \dots \\ V_{\mathrm{SR},N} \\ V_{\mathrm{SR},N} \end{bmatrix} \begin{matrix} \\ \} 1 \\ \\ \} 2 \\ \\ \} \dots \\ \\ \} N \end{matrix} \tag{10}$$

that is, both wires of the nth TWP carry the same voltage sources $V_{\mathrm{SL},n}$ and $V_{\mathrm{SR},n}$ at the left and right end, respectively. As a consequence, any DM component of noise sources within each TWP is neglected.

The application of a Thevenin-equivalent representation at the external ports leads to the following expressions of lumped voltage sources at section terminals [9], [10], [17]

$$V_{\mathrm{SL},n} = \int_0^{\mathscr{L}_i} \frac{\sin[\beta_0(z-\mathscr{L}_i)]}{\sin(\beta_0\mathscr{L}_i)} E_z(h_n,0,z)dz - \int_0^{h_n} E_x(x,0,0)dx \tag{11}$$

$$V_{\mathrm{SR},n} = \int_0^{\mathscr{L}_i} \frac{\sin(\beta_0 z)}{\sin(\beta_0\mathscr{L}_i)} E_z(h_n,0,z)dz - \int_0^{h_n} E_x\left(x,0,\mathscr{L}_i\right)dx. \tag{12}$$

For the computation of these integrals, the vertical components of the field are approximated by constant values as

$$E_x(x,0,0) \cong E_{x,\mathrm{RE}}(0) + jE_{x,\mathrm{IM}}(0)\ \forall x \tag{13}$$

$$E_x(x,0,\mathscr{L}_i) = E_{x,\mathrm{RE}}(\mathscr{L}_i) + jE_{x,\mathrm{IM}}(\mathscr{L}_i)\ \forall x \tag{14}$$

whereas the longitudinal component of the field is approximated by a piecewise-linear function of z as

$$E_z(h_n,0,z) \cong \chi_n[(az+b)+j(cz+d)] \tag{15}$$

$$a = [E_{z,\mathrm{RE}}(\mathscr{L}_i) - E_{z,\mathrm{RE}}(0)]/\mathscr{L}_i \tag{16}$$

$$b = E_{z,\mathrm{RE}}(0) \tag{17}$$

$$c = [E_{z,\mathrm{IM}}(\mathscr{L}_i) - E_{z,\mathrm{IM}}(0)]/\mathscr{L}_i \tag{18}$$

$$d = E_{z,\mathrm{IM}}(0) \tag{19}$$

$$\chi_n = h_n/h. \tag{20}$$

The linear-interpolation scheme in (15)–(19) is made clear in the upper plot of Fig. 2. The adimensional coefficient (20) is introduced in (15) to correct the field value sampled at the bundle height h so to approximate the field at each height h_n of the nth TWP. Indeed, the horizontal component of the electric field is approximately proportional to the height above a perfectly conducting ground if $h_n << \lambda$.

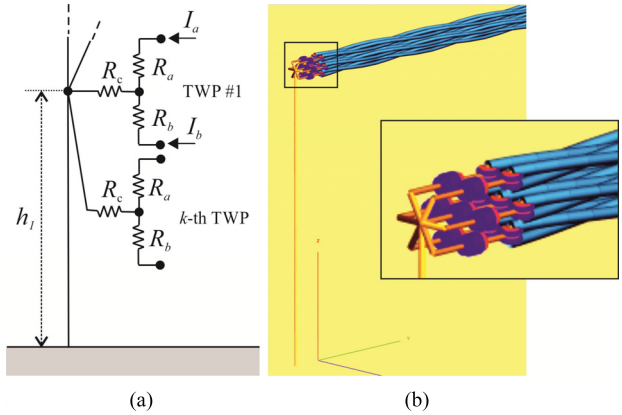

Fig. 4. Structure of terminal loads: (a) circuit model and (b) implementation in the full-wave MoM solver.

By inserting (13)–(20) into (11)–(12), voltage sources can be cast into closed form as

$$V_{\mathrm{SL},n} = (a+jc)\Sigma_L + (b+jd)\Psi_L - [E_{x,\mathrm{RE}}(0) + jE_{x,\mathrm{IM}}(0)]h_n \tag{21}$$

$$V_{\mathrm{SR},n} = (a+jc)\Sigma_R + (b+jd)\Psi_R - [E_{x,\mathrm{RE}}(\mathscr{L}_i) + jE_{x,\mathrm{IM}}(\mathscr{L}_i)]h_n \tag{22}$$

where

$$\Sigma_L = \frac{\sin(\beta_0\mathscr{L}_i) - \beta_0\mathscr{L}_i}{\beta_0^2\sin(\beta_0\mathscr{L}_i)} \tag{23}$$

$$\Sigma_R = \frac{\sin(\beta_0\mathscr{L}_i) - \beta_0\mathscr{L}_i\cos(\beta_0\mathscr{L}_i)}{\beta_0^2\sin(\beta_0\mathscr{L}_i)} \tag{24}$$

$$\Psi_{\substack{L\\R}} = \pm\frac{\cos(\beta_0\mathscr{L}_i) - 1}{\beta_0\sin(\beta_0\mathscr{L}_i)}. \tag{25}$$

Finally, the circuit model of the whole bundle is constructed by cascading the N_S circuit models of subsequent bundle sections, and it can be used, together with a multiport representation of terminal loads, to evaluate induced voltages and currents.

IV. Model Validation Versus Full-Wave Simulation

In this section, validity of the proposed model is assessed versus a reference full-wave solution obtained by the MoM-based software FEKO [18]. Without loss of generality, the bundle under analysis is composed of seven TWPs as in Fig. 1(a), and is characterized by the following data: $r_w = 0.15$ mm, $s = 0.7$ mm, $s_b = 1.5$ mm. Each TWP contains 40 twists having pitch 2.5 cm, therefore, the bundle length is $\mathscr{L} = 1$ m. For every TWP in the bundle, terminal loads at both ends have a general T configuration involving resistors R_a, R_b, R_c as shown in Fig. 4(a).

The whole bundle and terminal loads have been meshed with about 4000 wire segments in the MoM solver. A detail of the left termination is shown in Fig. 4(b). For a consistent comparison of results, such terminal structures modeled by wires in MoM cannot be treated as ideal resistive circuits in an MTL model,

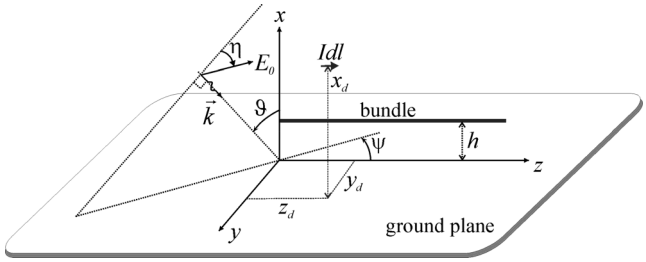

Fig. 5. Parameters of the plane wave and the Hertzian dipole.

not only because they show a frequency-dependent impedance, but also because they contribute to field coupling. Specifically, the dominant effect is given by the so-called vertical riser, i.e., the highest vertical segment of the length h_1 shown in Fig. 4(a). Therefore, the proposed bundle model has been implemented in conjunction with a transmission-line model of vertical risers whose details are reported in [19].

In order to provide well-defined and reproducible test cases for assessing model validity, the reported simulations refer to two canonical electromagnetic environments: 1) a plane-wave field and 2) a nonuniform field generated by a Hertzian dipole above ground. Indeed, in these cases, the electric field samples to be input in the proposed MTL model (see Section II-A) can be evaluated by means of closed-form exact solution of Maxwell equations. Hence, the obtained results are not affected by additional errors due to approximations involved in numerical computation of the incident field.

Electrical and geometrical parameters of the plane wave and the dipole are sketched in Fig. 5. The plane-wave field is characterized by the electric field strength E_0, incidence angles ϑ and ψ , and the polarization angle η. The Hertzian dipole is characterized by the product of current *I* times the length *dl,* and oriented parallel to the bundle in positions x_d, y_d, and z_d.

A. *Plane-Wave Field and Balanced Terminal Loads*

In the first test case, load resistors are perfectly balanced and equal to $R_a = R_b = 50\,\Omega$, $R_c = 100\,\Omega$. The incident field is the superposition of an impinging plane wave and the corresponding plane wave reflected by the ground plane. Specifically, the impinging wave has parameters: $E_0 = 1$ V/m, $\vartheta = 50°$, $\psi = 20°$, and $\eta = 60°$. The bundle height above the ground is $h = 5$ cm. Hence, the maximum frequency of interest is set to 600 MHz so that $h < \lambda/10$ (practical limit of validity for MTL models [2]). For field sampling, the bundle has been subdivided into $N_S = 50$ segments of equal length $\mathscr{L}_i = 2$ cm, so that $\mathscr{L}_i < \lambda/20$.

Predictions obtained by the proposed model are compared versus MoM simulations in Fig. 6. Specifically, the plotted quantities are the CM currents of different TWPs, defined as

$$I_{X,\mathrm{CM}} = I_a + I_b \tag{26}$$

where $X = L, R$ stands for the left and right terminals, respectively, and currents I_a and I_b are defined in Fig. 4(a). In order to find a tradeoff between completeness, conciseness of reporting, and plot readability, three TWPs at different heights above ground are considered in Fig. 6(a) for the left terminal, and other three in Fig. 6(b) for the right terminal. The obtained predictions are in remarkable agreement with MoM simulations with discrepancies generally limited to few decibels. Worst-case discrepancies in the order of 6 dBs are observed at the maximum frequency for the innermost TWP in the bundle (i.e., TWP #1) only.

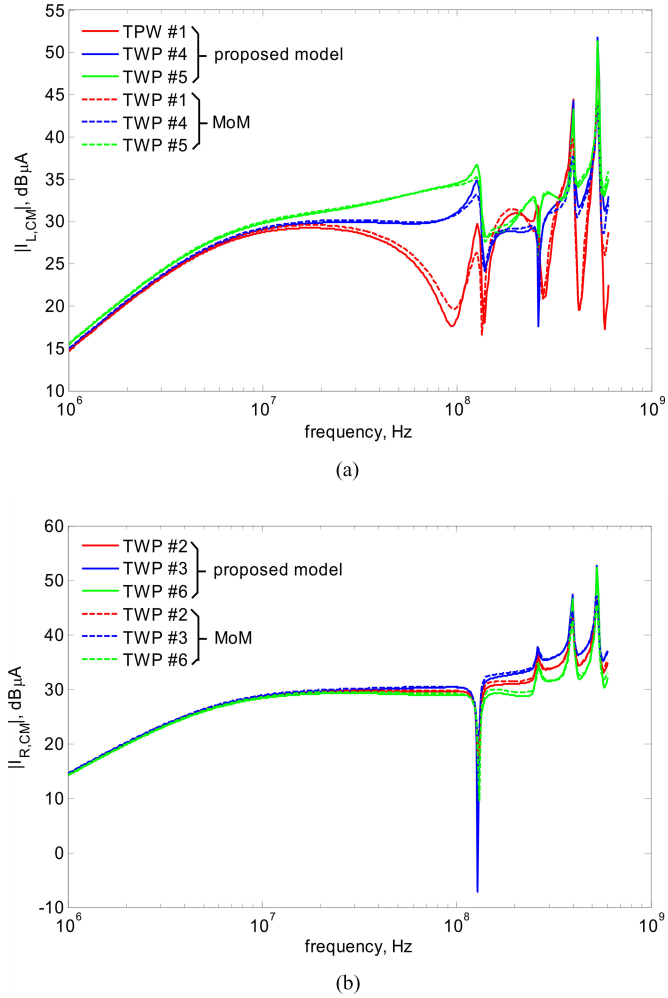

Fig. 6. Plane-wave field and balanced terminal loads: CM currents induced in terminal loads. Proposed model (solid line) versus MoM simulation (dashed line): (a) left end of TWPs #1, #4, and #5 and (b) right end of TWPs #2, #3, #6.

B. *Assessment of Validity Limits*

Model validity has been investigated through extensive simulations. An extreme and significant case is worth to be reported here, that is, when the bundle is placed at the minimum height above the ground according to the assumptions involved in the evaluation of averaged p.u.l. parameters (see Section II-B). In particular, results reported in Fig. 7 refer to the same setup described in Section IV-A, except for the choice of a very low bundle height $h = 3.4$ mm (such that TWPs #4 and #6 are at minimum allowed distance $h_4 = h_6 = 3\,s$ from ground). The

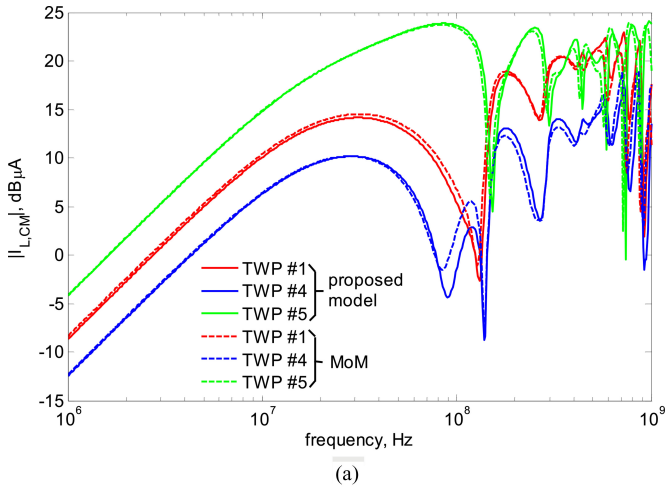

(a)

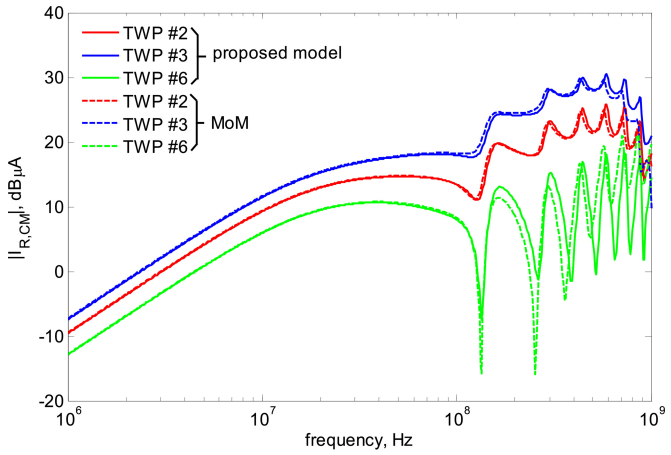

(b)

Fig. 7. Plane-wave field and balanced terminal loads: CM currents induced in terminal loads. Proposed model (solid line) versus MoM simulation (dashed line): (a) left end of TWPs #1, #4, and #5 and (b) right end of TWPs #2, #3, #6.

obtained predictions (solid curves in Fig. 7) result to be in fair agreement with MoM simulations (dashed curves in Fig. 7) with greater discrepancies for TWPs #4 and #6 as expected.

By inspecting several plots of simulation results, it has been found that the maximum frequency of validity $f_{\max}$ can be set according to the following rule of thumb:

$$\lambda_{\min} \cong \max(10\,h, 400\,s). \tag{27}$$

Namely, the minimum wavelength $\lambda_{\min} = c_0/f_{\max}$ is the greatest between two values. The former is the common limit of validity of MTL models ensuring dominant propagation of the transverse electro-magnetic mode [2], and holds for bundles running at a considerable height above ground (like for Section IV-A, Fig. 6, where $\lambda_{\min} \cong 50$ cm, and $f_{\max} \cong 600$ MHz). The latter is an additional frequency limit due to the approximation of a nonuniform MTL as a uniform MTL with averaged p.u.l. parameters, and is more restrictive than the former for bundles running at a short height $h < 40\,s$ above ground only (see the example in Fig. 7, where $\lambda_{\min} \cong 30$ cm, and $f_{\max} \cong 1$GHz).

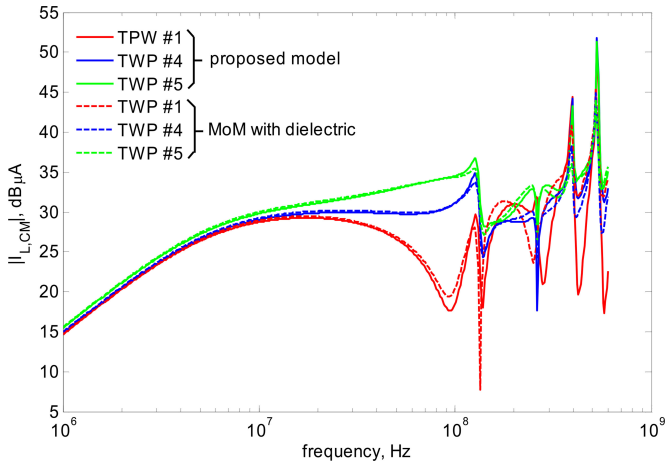

Fig. 8. Simulation used to show the impact of wire coating. CM currents induced at the left end of TWPs #1, #4, and #5 are computed via the proposed model (solid line, same curves of Fig. 6), and compared versus MoM simulations including dielectric coating of wires (dashed line).

C. Impact of Wire Coating

To show the influence of wire coating, the MoM simulation described in Section IV-A has been repeated by including dielectric jackets of wires with electric permittivity $\varepsilon_r = 3.5$ and thickness $t = r_w = 0.5$ mm. In Fig. 8, the obtained CM currents are compared versus those predicted by the proposed model, which neglects wire coating.

Comparison between Figs. 6(a) and 8 indicates that the dielectric plays a role only on the innermost TWPs (e.g., TWP #1), whereas discrepancies are negligible for the external TWPs (e.g., TWP #4 and #5). The effect of dielectric coating is limited to the resonance region of the bundle, and mainly concerns the depth of the notches of the frequency response. It is worth noting that its influence in terms of frequency shift is inconsequential as the proposed model focuses on CM excitation (whose phase velocity is very close to the speed of light in air).

D. Plane-Wave Field and Unbalanced Terminal Loads

Though the proposed model neglects any DM contribution to noise sources, it can account for the DM noise induced at terminal loads as a result of CM-to-DM conversion in case of unbalanced loads [11]–[14]. As an example, the same setup described in Section IV-A is considered here, except for the introduction of a 10% degree of imbalance affecting all terminal loads (this was achieved by setting different resistors $R_a = 45$ Ω, $R_b = 55$ Ω). DM currents, i.e.,

$$I_{X,\mathrm{DM}} = (I_a - I_b)/2 \tag{28}$$

where $X = L, R$, predicted by the proposed model are compared versus those obtained by MoM simulations in Fig. 9.

Results are in good agreement with MoM simulations in the lower frequency range. Discrepancies are more consistent above 200 MHz, as the contribution of pure DM noise (neglected in the proposed model) becomes no longer negligible with respect to the contribution due to CM-to-DM conversion [9, Sec. VI-C].

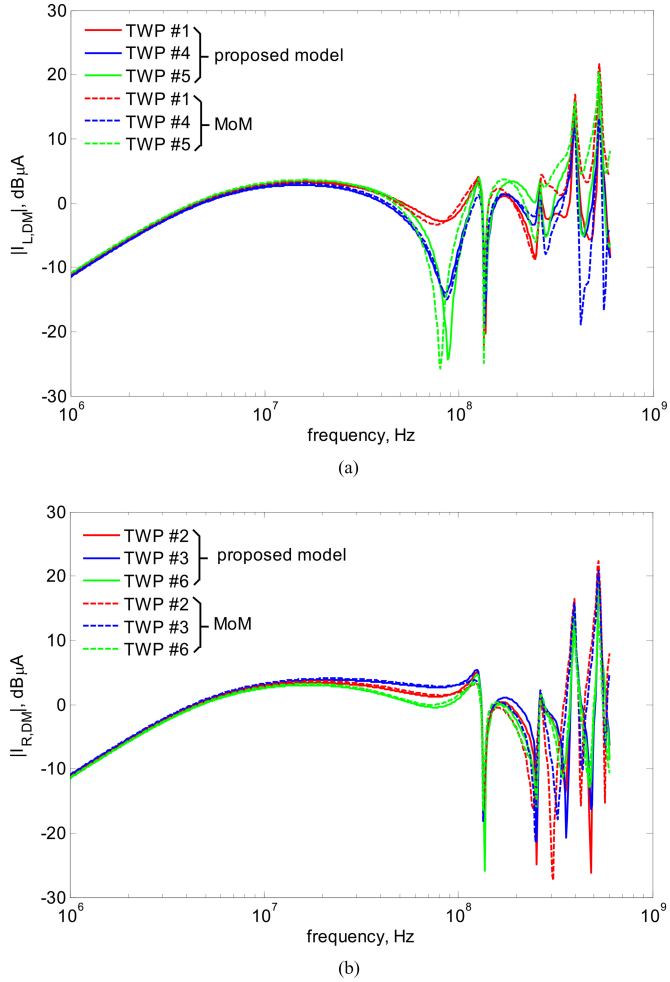

Fig. 9. DM currents induced in unbalanced terminal loads. Proposed model (solid line) versus MoM simulations (dashed line): (a) left end of TWPs #1, #4, and #5 and (b) right end of TWPs #2, #3, #6.

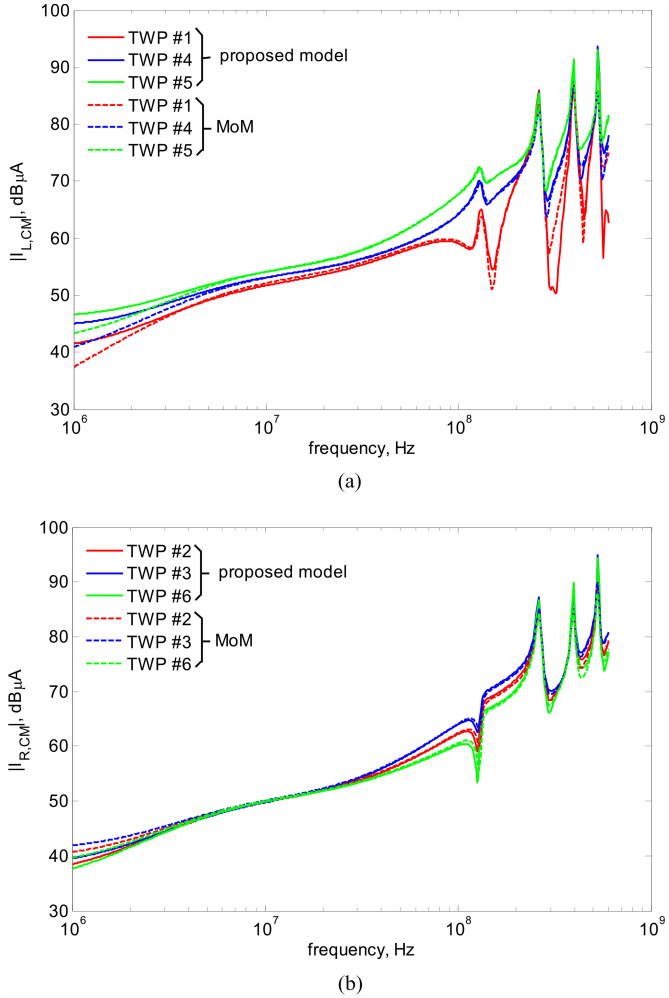

Fig. 10. Hertzian dipole and balanced terminal loads: CM currents induced in terminal loads. Proposed model (solid line) versus MoM simulations (dashed line): (a) left end of TWPs #1, #4, and #5 and (b) right end of TWPs #2, #3, #6.

E. Hertzian Dipole and Balanced Terminal Loads

The final example concerns the excitation of the bundle described in Section IV-A by means of a z-oriented Hertzian dipole above the ground instead of a plane wave. The dipole is characterized by $I\,dl = 1$ Am, $x_d = y_d = 1$ m, and $z_d = 0.25$ m.

CM currents induced at bundle terminals are plotted by solid curves in Fig. 10, and compared versus MoM simulations (dashed curves). Results are in good agreement. Discrepancies at very low frequencies are due to the high nonuniformity of the incident electric field. Indeed, since the near-field region of the Hertzian dipole, characterized by high field gradients, is larger at lower frequencies, the approximations used for field interpolation [see (13)–(20)] result to be less accurate than for higher frequencies.

V. Conclusion

An approximate MTL model for RS prediction of bundles composed of TWPs running above the ground has been developed. The model accounts for CM excitation of each TWP in the bundle due to the presence of an incident nonuniform electromagnetic field, and can be used to accurately predict (a) the CM noise induced at the terminals of each TWP and (b) the DM induced at the terminals of each TWP due to load imbalance and consequent CM-to-DM conversion.

Simulation results presented in Section IV (see Figs. 6, 7, and 10) have shown that the CM current considerably differs from one TWP to another in the bundle, even if all TWPs have the same terminal loads, due to different positioning in the cross section. Particularly, the innermost TWPs (e.g., TWP #1 in Fig. 6), and those closer to ground (e.g., TWP #4 and #6 in Fig. 7) benefit from the shielding effect played by the surrounding wires, since CM currents induced at their terminals are generally lower than those of other pairs. Additionally, remarkable differences in the induced current levels of TWPs (tens of decibels) are found when the bundle is very close to ground (see Fig. 7). Unlike for the analysis of radiated emissions, for which the knowledge of the CM current of the whole bundle suffices, the above differences stress that predicting the CM current in every single TWP is of paramount importance for RS analysis.

Furthermore, the computational burden for the proposed model is much lower than for full-wave solvers. As an example, MoM solutions (500 frequency points) reported in Fig. 6 required more than 4 h of run-time on a six-core CPU Intel i7 3.33 GHz equipped with 24-GB RAM, whereas results were obtained in few seconds via the proposed model. Finally, since the input consists of a set of field samples, the proposed model can be integrated in any full-wave solver used to compute the incident electromagnetic field, leading to a computationally efficient simulation tool for the prediction of RS in complex electromagnetic environments.

APPENDIX

For the approximation of integrals (2)–(4), the involved p.u.l. inductances are first expressed in the closed form for widely separated wires [2, ch. 5.2], and then approximated by series expansions. The terms of the series retain the dependence on φ_n and can be easily integrated.

As an example, the following Taylor series for $\chi = s/h_n = 0$ is used to approximate inductance l_n in (2)

$$l_n(\chi, \varphi_n) = l_n(0, \varphi_n) + l'_n(0, \varphi_n)\chi + 0.5 l''_n(0, \varphi_n)\chi^2 + \dots \tag{A1}$$

where l'_n, l''_n, etc., denote derivatives with respect to variable χ. A similar approach is used to approximate inductance l_{nk} in (4). For the mutual inductance $l_{M,n}$ in (3), which exhibits a singularity in $\chi = 0$, the following expansion is used:

$$\begin{aligned} l_{M,n} &= \frac{\mu_0}{4\pi} \ln\left(\sin^2\varphi_n + \frac{4}{\chi^2}\right) \\ &\approx \frac{\mu_0}{4\pi}\left[\ln\left(\frac{4}{\chi^2}\right) + \frac{\chi^2}{4}\sin^2\varphi_n \ -\frac{\chi^4}{32}\sin^4\varphi_n + ...\right]. \end{aligned} \tag{A2}$$

The series is truncated in (5)–(7) to retain only significant terms that lead to accurate results (error less than 1%) under the reported geometrical constraints.

REFERENCES

[1] C. Jullien, P. Besnier, M. Dunand, and I. Junqua, "Advanced modeling of crosstalk between an unshielded twisted pair cable and an unshielded wire above a ground plane," *IEEE Trans. Electromagn. Compat.*, vol. 55, no. 1, pp. 183–194, Feb. 2013.

[2] C. Paul, *Analysis of Multiconductor Transmission Lines*. New York, NY, USA: Wiley Interscience, 1994.

[3] A. K. Agrawal, H. J. Price, and S. H. Gurbaxani, "Transient response of multiconductor transmission-lines excited by a nonuniform electromagnetic field," *IEEE Trans. Electromagn. Compat.*, vol. EMC-22, no. 2, pp. 119–129, May 1980.

[4] M. Leone and H. L. Singer, "On the coupling of an external electromagnetic field to a printed circuit board trace," *IEEE Trans. Electromagn. Compat.*, vol. 41, no. 4, pp. 418–424, Nov. 1999.

[5] P. Manfredi and F. G. Canavero, "Polynomial chaos for random field coupling to transmission lines," *IEEE Trans. Electromagn. Compat.*, vol. 54, no. 3, pp. 677–680, Jun. 2012.

[6] M. Omid, Y. Kami, and M. Hayakawa, "Field coupling to uniform and nonuniform transmission lines," *IEEE Trans. Electromagn. Compat.*, vol. 39, no. 3, pp. 201–211, Aug. 1997.

[7] A. Shoory, M. Rubinstein, A. Rubinstein, C. Romero, N. Mora, and F. Rachidi, "Application of the cascaded transmission line theory of Paul and McKnight to the evaluation of NEXT and FEXT in twisted wire pair bundles," *IEEE Trans. Electromagn. Compat.*, vol. 55, no. 4, pp. 648–656, Aug. 2013.

[8] C. R. Paul and M. B. Jolly, *Crosstalk in twisted-wire circuits*, Rome Air Development Center, Griffiss AFB, Rome, NY, USA, Tech. Rep. RADC-TR-82–286, vol. IV-C, Nov. 1982.

[9] S. A. Pignari and G. Spadacini, "Plane-wave coupling to a twisted-wire pair above ground," *IEEE Trans. Electromagn. Compat.*, vol. 53, no. 2, pp. 508–523, May 2011.

[10] G. Spadacini and S. A. Pignari, "Numerical assessment of radiated susceptibility of twisted-wire pairs with random nonuniform twisting," *IEEE Trans. Electromagn. Compat.*, vol. 55, no. 5, pp. 956–964, Oct. 2013.

[11] F. Grassi, G. Spadacini, S. A. Pignari, "The concept of weak imbalance and its role in the emissions and immunity of differential lines," *IEEE Trans. Electromagn. Compat.*, vol. 55, no. 6, pp. 1346–1349, Dec. 2013.

[12] F. Grassi and S. A. Pignari, "Bulk current injection in twisted-wire pairs with not perfectly balanced terminations," *IEEE Trans. Electromagn. Compat.*, vol. 55, no. 6, pp. 1293–1301, Dec. 2013.

[13] F. Grassi and S. A. Pignari, "Immunity to conducted noise of data transmission along DC power lines involving twisted-wire pairs above ground," *IEEE Trans. Electromagn. Compat.*, vol. 55, no. 1, pp. 195–207, Feb. 2013.

[14] F. Grassi, G. Spadacini, and S. A. Pignari, "SPICE behavioral modeling of RF Current injection in wire bundles," *IEICE Trans. Commun.*, vol. E97-B, no. 2, pp. 424–431, Feb. 2014.

[15] A. Sugiura and Y. Kami, "Generation and propagation of common-mode currents in a balanced two-conductor line," *IEEE Trans. Electromagn. Compat.*, vol. 54, no. 2, pp. 466–473, Apr. 2012.

[16] G. Spadacini, D. Bellan, and S. Pignari, "Impact of twist non-uniformity on crosstalk in twisted-wire pairs," in *Proc. IEEE Symp. Electromagn. Compat.*, Boston, MA, USA, Aug. 18–22, 2003, pp. 483–488.

[17] G. Spadacini, S. A. Pignari, and F. Marliani, "Closed-form transmission line model for radiated susceptibility in metallic enclosures," *IEEE Trans. Electromagn. Compat.*, vol. 47, no. 4, pp. 701–708, Nov. 2005.

[18] *FEKO Suite 6.3 User's Manual*. (Oct. 2013). © EM Software and Systems, S. A.(Pty) Ltd., Stellenbosch, South Africa [Online]. Available: www.feko.info

[19] S. A. Pignari and D. Bellan, "Incorporating vertical risers in the transmission line equations with external sources," in *Proc. IEEE Int. Symp. Electromagn. Compat.*, Santa Clara, CA, USA, Aug. 9–13, 2004, pp. 974–979.